Developing novel gas sensors for NO_2 detection based on $Ce_{(1-x)}M_XO_2$, {M=Ru, In} solid solutions

**Ricardo Rangel · Lidia Chávez-Chávez ·
Manuel García-Méndez · Eduardo Martínez**

Abstract CeO_2, $Ce_{(1-x)}M_XO_2$, {M=Ru, In} compounds with sensing properties were fabricated using the sol–gel route. The main purpose was to compare the efficiency of CeO_2 vs. $Ce_{(1-x)}M_XO_2$ doped compounds as gas sensors for NO_2 detection. Characterization was performed by means of X-ray diffraction (XRD), scanning electron microscopy (SEM) and surface area determination (BET). Measurements of electrical resistance under different conditions of time, concentration and temperature in the presence of NO_2 were carried out. Ruthenium inclusion increased the CeO_2 sensor response in a great extent, gas response (S)=1.8 for CeO_2 vs. gas response (S)=350 for $Ce_{0.95}Ru_{0.05}O_2$ and gas response (S)=35 for $Ce_{0.95}In_{0.05}O_2$. This behavior is reported by the first time. Our results demonstrate that ruthenium or indium inclusion has been beneficial for CeO_2. Conclusively the materials herein described could be applied as NO_2 gas sensors.

Keywords Gas sensors · Semiconductors · Solid solutions · Cerium oxide · Ceria · Mixed oxides

1 Introduction

Design, application and development of new gas sensors have drawn great technological interest in recent years. Their justification is held in areas such as medicine, automotive industry (detectors for CO_x, NO_x, SO_x gases), industrial waste gases, volatile organic compounds (VOC), hydrocarbons, and ozone detection, to name a few. Currently, there is a large number of materials that exhibit suitable properties for gas sensor applications, mostly based on SnO_2, SnO_2-Sb, ZnO, CuO, CuO_2, Ga_2O_3, GaN, WO_3 and mixtures thereof [1–3]. Their sensorial response is a function of large number of variables such as size, shape, growth conditions; and mainly chemical composition, which makes their study very complex. On that context cerium oxide (CeO_2) is a promising new candidate as a gas sensor compound [3, 4] and the reasons are discussed below.

The mechanism followed by CeO_2 during gas detection is different to that common semiconductor sensors are usually based on. For semiconducting materials, the detection process is based mostly on reactions occurring at the surface. Usually, the available oxygen is adsorbed on the surface dangling bonds. Thus, an electron of the conduction band is transferred and the electrical conductance of the material experiences a reduction [5]. In contrast, CeO_2 exhibits relatively high oxygen mobility on its surface and also inside the lattice (bulk level) at elevated temperature.

R. Rangel (✉) · L. Chávez-Chávez
División de Estudios de Posgrado, Facultad de Ingeniería Química,
Universidad Michoacana de S.N.H,
Morelia, Michoacán, México
e-mail: rrangel@umich.mx

M. García-Méndez
Facultad de Ciencias Físico-matemáticas,
Universidad Autónoma de Nuevo León,
Cd. Universitaria,
San Nicolás de los Garza, NL, México

M. García-Méndez
CIIDIT-UANL,
Apodaca, Nuevo León, México

E. Martínez
CIMAV, S.C.,
Parque de Investigación e Innovación Tecnológica (PIIT),
Nueva Carretera Aeropuerto Km. 10,
Apodaca, Nuevo León, México

Ceria has been recognized as a key material of the three-way catalysts in automobiles since it can release and uptake oxygen accordingly to the general reversible expression [6]:

$$CeO_2 = CeO_{2-x} + x/2O_2 \qquad (1)$$

The amount of oxygen released (left-to-right) or stored (right-to-left) is generally referred to as oxygen storage capacity (OSC).

Cerium oxide (IV) has a face centered cubic fluorite-type cell in which each cerium ion is coordinated by eight oxygen neighbors. These extremely open structures tolerate a high level of atomic disorder, which can be induced by doping [7, 8]. An important effect of the cation doping is to increase the formation of defects like oxygen vacancies that lead to a higher oxygen storage capacity (OSC) according to the Eq. 1. Thus, the incorporation of aliovalent elements into the CeO_2 lattice produces lattice oxygen anion vacancies by a charge-compensating effect of foreign cations as follows:

$$xMO + (1-x)\,CeO_2 \leftrightarrow xM_{Ce}^{''} + xV_O^{\bullet\bullet} + (1-x)\,Ce_{Ce} + (2-x)O_O \qquad (2)$$
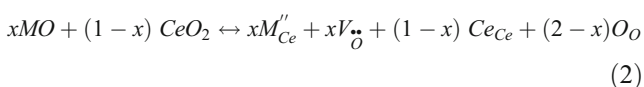
Where M in Eq. 2 might be a divalent (M^{2+}) or trivalent (M^{3+}) cation, (for instance La^{3+}, In^{3+} or Ru^{2+}), V_δ is an oxygen anion vacancy. Therefore when reduction occurs, both vacancies and electrons can be observed [9].

$$O_O \leftrightarrow \frac{1}{2}O_2 + V_O^{\bullet\bullet} + 2e^{'} \qquad (3)$$

In this context, lanthanum [7], indium [10–14] and ruthenium [15, 16], are elements that have been successfully tested as oxides for some applications like gas-sensor materials and in the present work, are added to ceria.

Based on these analyses, the present work proposes the application of ceria mixed compounds, doped either with Ru or In as gas sensor materials. The main purpose is to compare the efficiency of CeO_2 vs. $Ce_{(1-x)}M_xO_2$ doped materials for NO_2 detection. Our hypothesis is that partial substitution of cerium by Ru or In to produce $Ce_{(1-x)}Ru_xO_2$ and $Ce_{(1-x)}In_xO_2$ solid solutions can lead to a defective lattice, increasing oxygen conductivity with possible additional electronic states which may be positive for their development as gas sensors.

We expect to contribute to the development of new sensor structures that can be produced with adequate reproducibility, stability and operability in a wide range of temperatures.

2 Experimental

2.1 Sample preparation

Samples were prepared by the sol–gel method by means of the citric acid route, starting with $C_6H_9O_6In$, $Ru_3(CO)_{12}$ and $Ce(C_2H_3O_2)_3 \cdot 1.5H_2O$ compounds, dissolved in water or isopropyl alcohol and stirred for 4 h at constant temperature (80°C) to obtain the sol and later, the mixture was evaporated slowly to form the gel (110°C for 12 h). Finally, when a fluffy solid was obtained, it was burned at 600°C for 4 h with a heating ramp of 5°C/min. After that, the system was left to slow cool.

2.2 Characterization

The systems under study were characterized by X-ray diffraction method using a Siemens D-5,000 model, operating at 30 kV and 20 mA, Cu K_α radiation with a step size of 0.02 ° (deg)/min from 10 to 70 ° (2θ). Microscope images were obtained in an SEM JSM-6400 JEOL Noran Instrument, at 20 kV and 10^{-6} Torr. BET surface was measured in Micrometrics Gemini 2060 RIG-100 model with nitrogen adsorption at 77 K. Thermal Gravimetric Analysis (TGA) was performed using a Universal TA instrument, model SDT Q600 under N_2 flow.

2.3 Sensing films preparation

The gas sensors were fabricated by spin coating the slurry of synthesized CeO_2 and $Ce_{(1-x)}M_XO_2$ doped compounds on the cleaned alumina substrates, which were attached to a pair of interdigitated Pt electrodes with a thickness of 100 nm. (see Fig. 1(b)). The electrodes were deposited using RF magnetron sputtering method. The coating slurry was prepared by ultrasonically dispersing CeO_2, $Ce_{0-95}In_{0.05}O_2$, $Ce_{0.95}Ru_{0.05}O_2$ powders in mixed organic solvents of terpineol and ethanol with 2:1 volume ratio for 1 h. To avoid the presence of slurry at the end of the substrate a physical mask was used during spin coating. The coated sensing films were dried in air for 30 min and subsequently annealed at 200°C for 1 h at ambient atmosphere in order to burn out the organic solvent used in preparation of coating paste and to enhance the adherence of the sensing film to the sensor substrates. Afterwards the temperature was raised to 300°C using a slow ramp of 1°C/min in order to avoid the eventual appearance of cracks in the films.

2.4 Experimental setup

The NO_2 gas sensing measurements were carried out in a computer-controlled static gas sensing characterization system provided with an array of data acquisition.

The electrical resistance of CeO_2 was measured as a function of time according to the experimental setup of Fig. 1. Resistance was measured under a flow of 1 to 10 ppm using NO_2 as testing gas (see Fig. 2). The gas concentration was controlled adjusting the flow rates. Synthetic air was used as carrier gas to ensure constant total flow rate of 100 mL/min.

Fig. 1 (a) Work gas testing station system, (b) Schematic layout of alumina substrates and experimental setup. On the top right: back side of the substrate with the platinum heater and front side of the substrate with the interdigitate electrodes
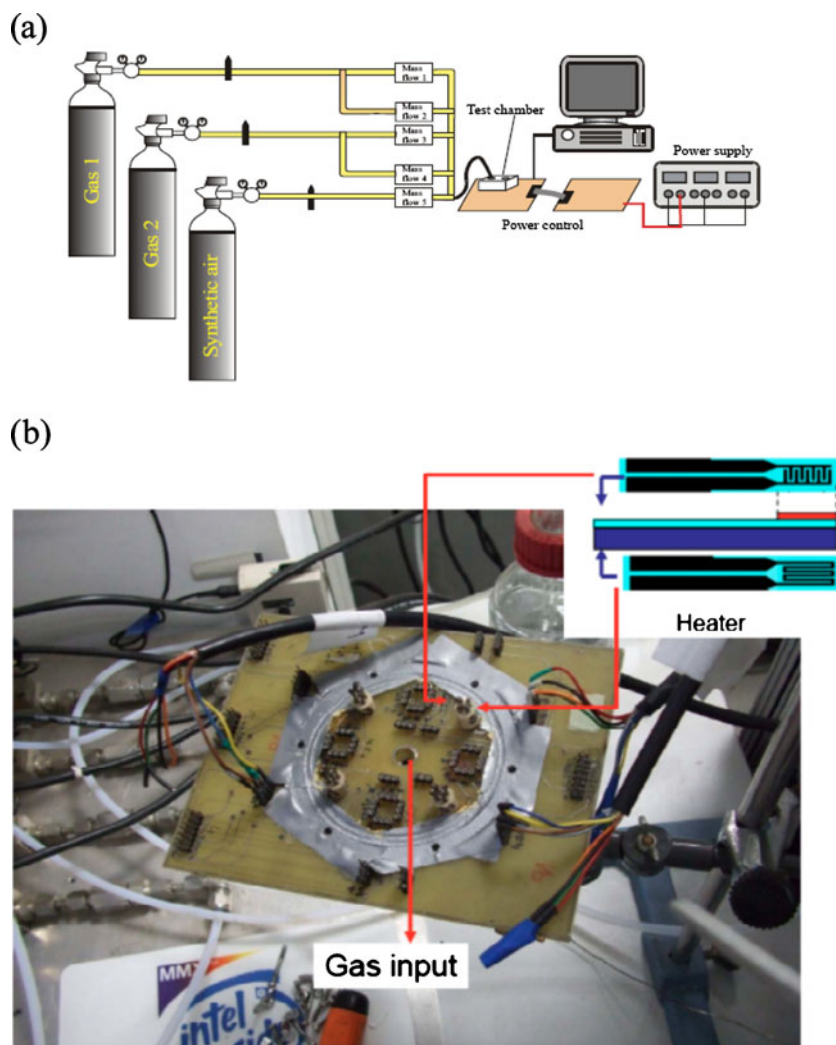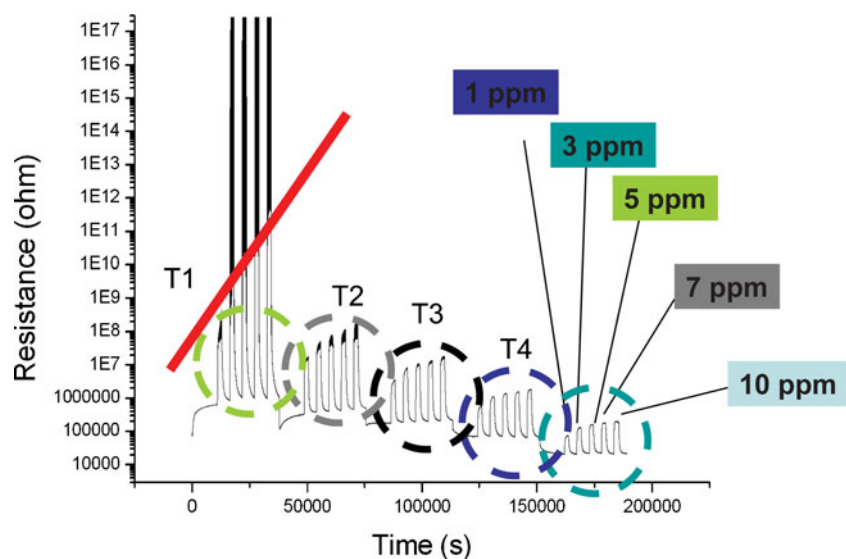

Fig. 2 Schematic drawing of electrical resistance response as a function of temperature and gas concentration of 1, 3, 5, 7, and 10 ppm using NO_2 as a testing gas for $Ce_{0.95}Ru_{0.05}O_{2+/-\delta}$ compound. Working temperatures $T_i = 200, 250, 300, 350$ and $400°C$

Different samples were exposed to nitrogen dioxide (NO_2) at several concentrations and temperatures according to the general diagram shown on Figs. 1(a,b) and 2. NO_2 gas was tested at fixed temperature under steady state and transient modes between 150°C and 450°C using a flow-type measurement cell. The gas response for every sample is defined as the R_{gas}/R_{air} ratio for NO_2, where R_{air} represents the electrical resistance for every material measured under synthetic air while R_{gas} represents the resistance during gas exposure. The response time is defined as the time required for the resistance to rise up to 90% of the equilibrium value since the test gas is injected. The gas was tested at five different temperatures and five concentrations.

3 Results and discussion

The crystal phase and crystallite size were established by means of X-ray diffraction analysis as shown in Fig. 3. From this analysis it is observed that $Ce_{(1-x)}Ru_xO_2$ and $Ce_{(1-x)}In_xO_2$ solid solutions are monophasic and isostructural to CeO_2 as observed in the diffraction pattern indexed in accordance with JCPDS 34–0394 card. From diffraction graphs, it is possible to observe peak broadening of the (111), (200), (220) and (311) reflections. This broadening indicates a decrease in crystallite size due to the added dopant. In order to verify this assumption, the crystal size was calculated for every system through the Scherrer equation [17]:

$$L = \frac{K\lambda}{W \cos \Theta} \qquad (4)$$

Here K is a constant which depends on the particle morphology, usually K=1.0; λ is the Cu, K_α radiation (nm); W is the
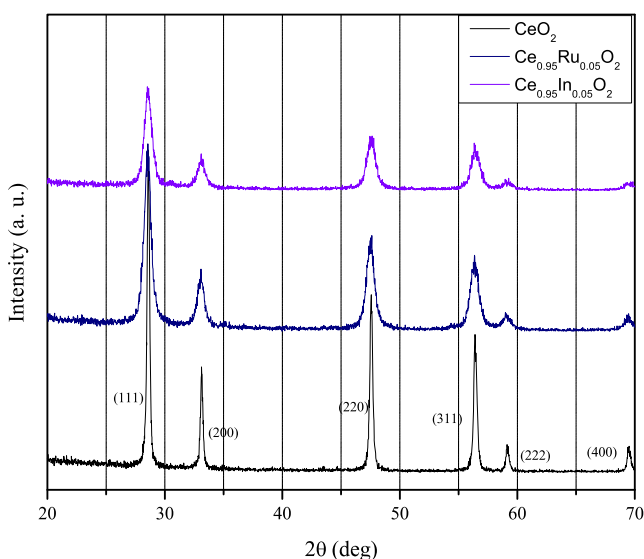

Fig. 3 XRD of CeO_2, $Ce_{0.95}In_{0.05}O_2$ and $Ce_{0.95}Ru_{0.05}O_2$ compounds synthesized at 700°C

full width at half-maximum (rad); Θ is the diffraction angle (deg). The (111) reflection index was used to perform the calculations using the Eq. 4. The calculated crystal sizes were 0.048, 0.018 and 0.016 μm for CeO_2, $Ce_{(1-x)}Ru_xO_2$ and $Ce_{(1-x)}In_xO_2$, respectively. From these values it is possible to establish that the inclusion of ruthenium and indium in the FCC lattice determines the decrease in the average crystal size in comparison with the one of CeO_2. The presence of secondary phases was not observed (for example RuO_2 or In_2O_3 oxides).

In addition to crystal size determination it was performed the calculation of the cell parameter, a for the FCC CeO_2 structure and also for $Ce_{0.95}Ru_{0.05}O_2$ and $Ce_{0.95}In_{0.05}O_2$ compounds. By combining the Bragg law with the plane spacing equation for the FCC cubic system, the following relation is readily obtained:

$$\frac{4 \sin^2\theta}{\lambda^2} = \frac{h^2 + k^2 + l^2}{a^2} \qquad (5)$$

In this way, is possible to calculate for a specific plane of reference, eg (111) of CeO_2 the a parameter value. The values obtained by using the Eq. 5 are as follows CeO_2=5.40, $Ce_{0.95}In_{0.05}O_2$=5.42 and $Ce_{0.95}Ru_{0.05}O_2$=5.43 Å. In such a case it is pertinent to conclude that crystal size and cell parameter are consistently affected by the doping process.

In order to compare real and stoichiometric composition, EDS microanalysis was carried out, finding good agreement with respect to the theoretical calculations within an error of 2%.

SEM analysis, included in Fig. 4, shows lengthened fibers. The apparent width is about 0.1 μm, with length ranging from 2 to 4 μm. The basic form of cerium oxide is uniform and the appearance of secondary phases does not seem evident in Fig. 4(b) and (c). This could indicate that the solubility limit of the $Ce_{1-x}M_xO_2$ compound was not exceeded since the occurrence of In_2O_3 (cubic) or RuO_2 (rhombohedral) is not observed. The fiber-like shape observed for all the samples is an additional positive factor related to the gas sensor properties Because they show a very large available surface area which could facilitate the sensing mechanism. As discussed previously by other authors crystal size and shape are properties directly related with the sensorial response [1–4].

Surface area was measured by means of BET method; from these measurements, a meaningful increase in the surface area of $Ce_{(1-x)}In_xO_2$ (10.2 m^2/g) and $Ce_{(1-x)}Ru_xO_2$ (13.4 m^2/g) was detected in comparison to CeO_2 (4.1 m^2/g). This result is remarkable, since the three compounds were prepared under the same experimental method. Thus, a correlation between surface area and sensorial response can be expected based on the fact that a larger value of surface area would exhibit more active sites anchored to the NO_2 molecule.

Fig. 4 SEM micrograph of (**a**) CeO$_2$, (**b**) Ce$_{0.95}$In$_{0.05}$O$_2$ and (**c**) Ce$_{0.95}$Ru$_{0.05}$O$_2$ samples. Notice that the three images have the same magnification, 5,000 X
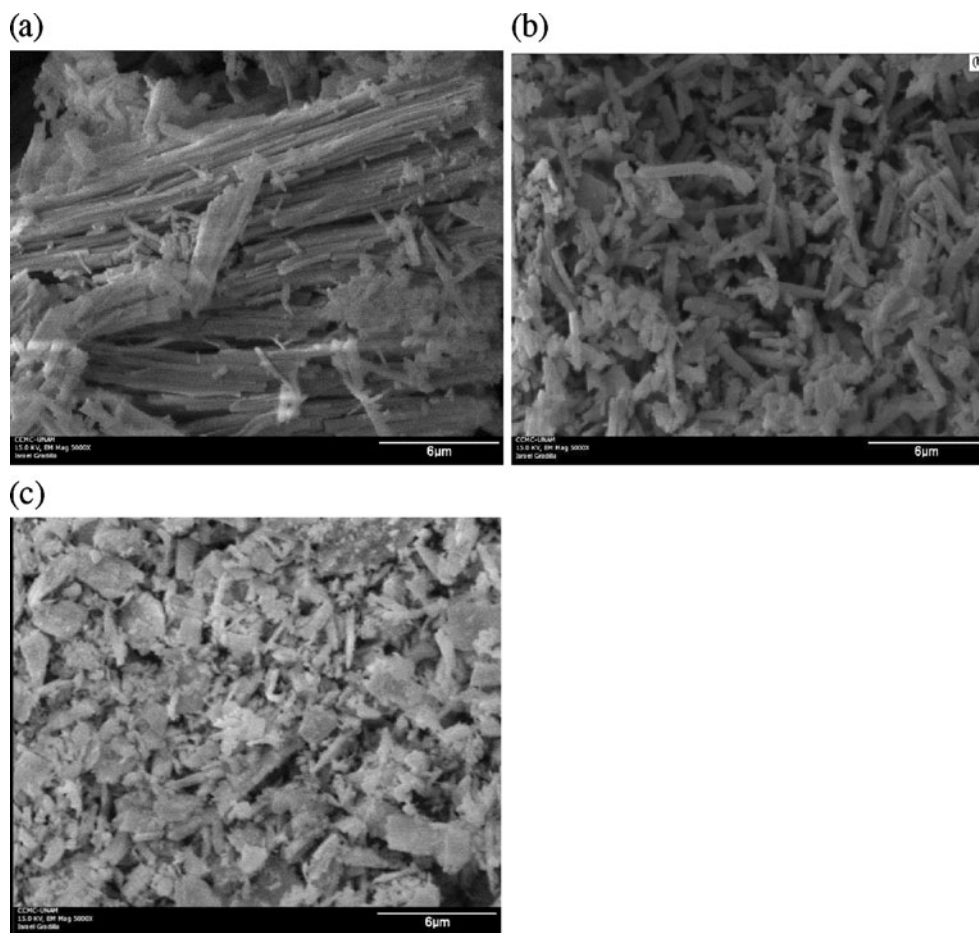
To reinforce our previous observations of the analysis by X-ray diffraction and scanning electron microscopy, thermo-gravimetric analyses were performed as shown in Fig. 5. The main objective was to identify whether the proposed systems formed RuO$_2$ or In$_2$O$_3$ in addition to Ce$_{0.95}$Ru$_{0.05}$O$_2$ or Ce$_{0.95}$In$_{0.05}$O$_2$ solid solutions.

The measurement range was from 50 to 1000°C for Ce$_{0.95}$In$_{0.05}$O$_2$ system while for Ce$_{0.95}$Ru$_{0.05}$O$_2$ compound it was 50 to 1600°C. Both under N$_2$ atmosphere as previously discussed. The sample weight was 37.17 mg for Ce$_{0.95}$Ru$_{0.05}$O$_2$ and 84.70 mg for Ce$_{0.95}$In$_{0.05}$O$_2$. Weight loss of the order of 1% to 2% was observed for each system, mainly due to the oxygen content variation or bound water.

In the case of indium or ruthenium oxide existed separately from the Ce$_{0.95}$Ru$_{0.05}$O$_2$ or Ce$_{0.95}$In$_{0.05}$O$_2$ solid solutions, to react with N$_2$ had occurred the formation of metallic ruthenium or indium. In this case, there would be an endothermic peak observed as a result of the transition from ruthenium oxide to metallic ruthenium (250°C). Simultaneously, we would have observed a decrease in the weight diagram, and this was not appreciated. Similar arguments can be explained for the case of indium oxide, for which the transition occurs at 219°C. Allowing the use of these solid solutions in the range of work considered as gas sensors in the present work.

Also the observations are consistent with the XRD analysis. Due to the range of work that we want to apply these sensor materials is not considered determinant if they are stable beyond 500°C, however important is that it was not observed any decomposition even above this temperature. Thus the results indicate that these compounds are stable and can be functional in the range of application of solid state-gas sensors.

4 Evaluation of sensor properties

A typical response transient of CeO$_2$ sample toward NO$_2$ gas balanced with air is shown in Fig. 6, and established as a reference material. The compound was exposed to NO$_2$ concentrations of 1, 3, 5, 7 and 10 ppm at 200, 250 and 300°C, as mentioned in the previous experimental section, (see Fig. 2 for definition of gas concentration and temperature steps). Upon injecting the NO2 gas, the resistance increased rapidly exhibiting the n-type semiconductor behavior, see Fig. 6(a). The experiment performed at 200°C for 300 min on CeO$_2$ showed that resistance values as a function of time are quite stable. It is observed that the value of resistance is located close to 1×10^9 ohms for all the
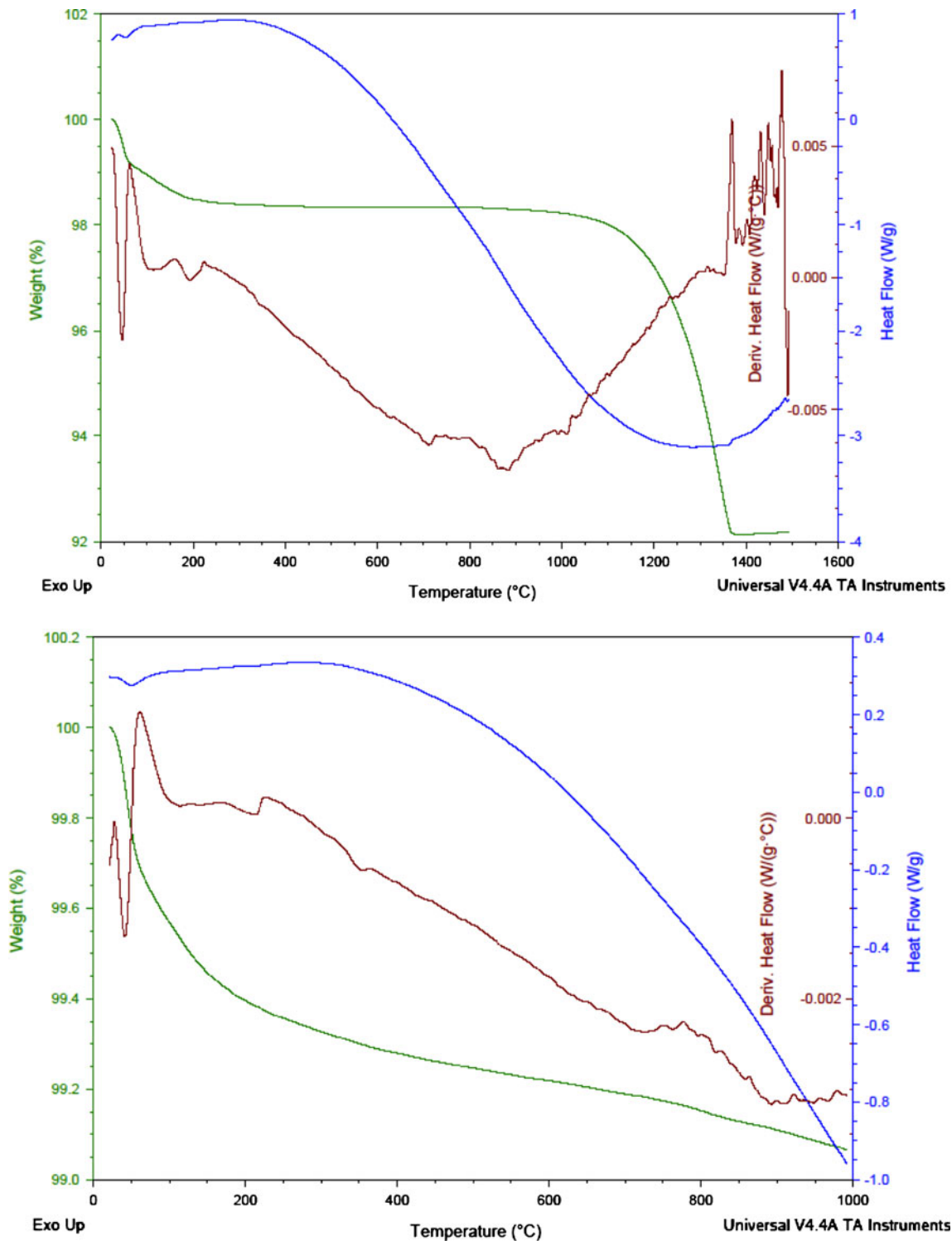
Fig. 5 Thermo-gravimetric analysis for $Ce_{0.95}Ru_{0.05}O_{2+/-\delta}$ (top), $Ce_{0.95}In_{0.05}O_{2+/-\delta}$ (bottom) solid solutions

concentrations. After completing the cycle of study at several concentrations, we started a new sequence for 300 min at a different temperature. It was found that following each cycle of measurements the resistance value diminishes by a factor of about 10 for the next cycle. The graph of gas response vs.

concentration, Fig. 6(b), shows a linear behavior with small variations within the studied range. Regarding gas response (S) vs. temperature, see Fig. 6(c), the values range between 1.4 and 1.7 at 200°C; S decreases to 0.95 near to 250°C and then increases to S=1.1 at 300°C. The response time ranges
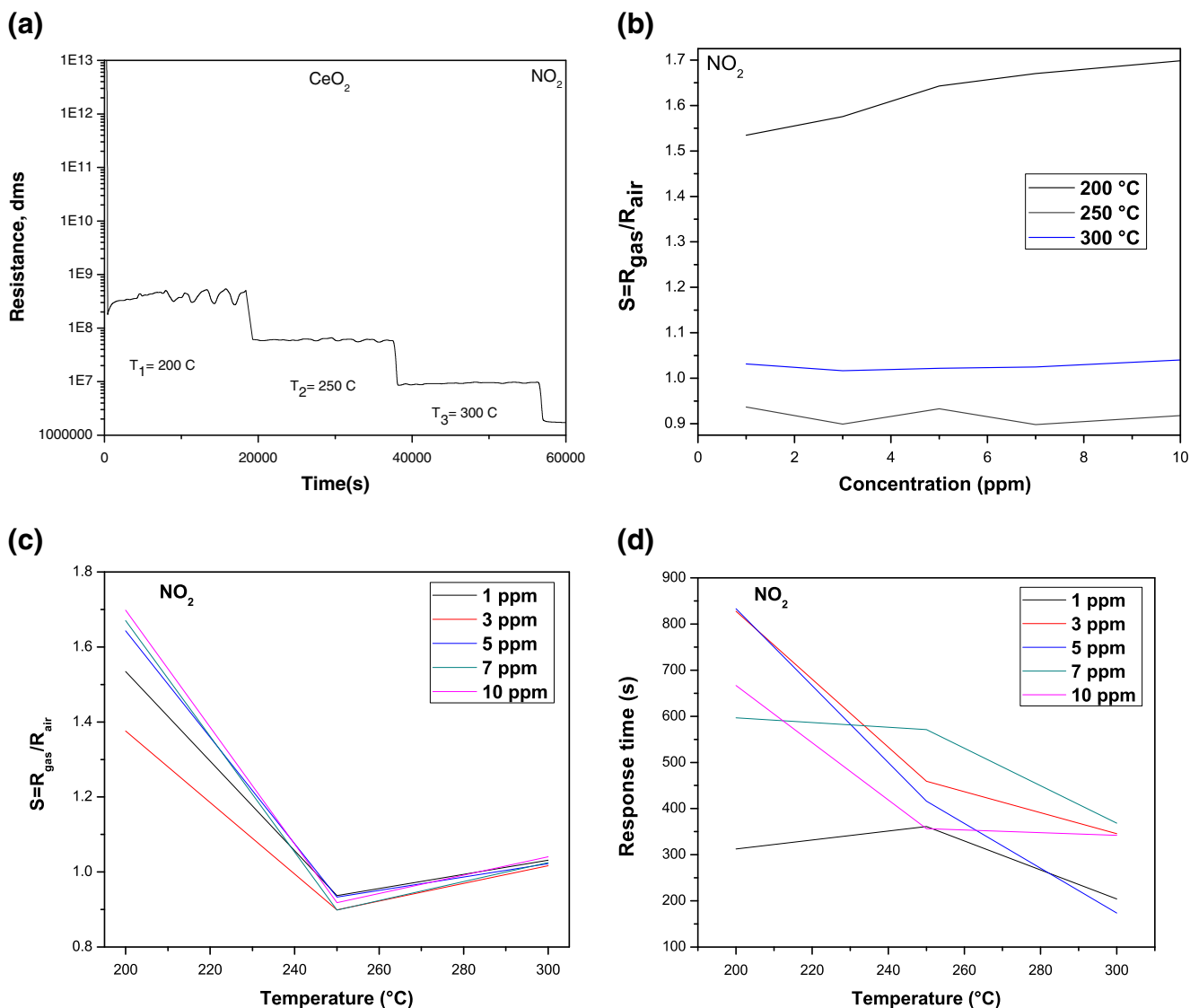
(a)

(b)

(c)

(d)

Fig. 6 CeO_2 graphs for (**a**) Resistance vs time, (**b**) Sensor response vs concentration, (**c**) Sensor response vs temperature, (**e**) Response time vs temperature

between 200 and 800 s at 200°C depending on the concentration under study, see Fig. 6(e). However, at higher temperature, close to 300°C, the response time ranges between 200 and 400 s, demonstrating that the sensor is more stable at higher temperatures. In general, a decrease in the response time at higher NO_2 concentrations was observed.

Concerning the recovery time as a function of temperature, it was observed that the time was shorter at working temperatures between 250°C and 300°C, whereas at low temperatures, near 200°C, the recovery time was longer. Somewhat surprising is that at 250°C the recovery time remains unchanged with a value of 300 s for all the concentration levels. The explanation can be as follows. Nearby 250°C, under O_2 flow the reaction $2CeO_2 \leftrightarrow Ce_2O_3 + \frac{1}{2}O_2$, takes place and CeO_2 is in equilibrium with Ce_2O_3 O_2 decomposes and the surface is rich in monatomic O and

NO_2. Consequently, thermal stability predominates and O and NO_2 adsorption are stable on the surface. As temperature increases, the surface becomes unstable, the frequency of vibration of dangling bonds at the surface also increases and NO_2 is desorbed.

Under NO_2 exposure the $Ce_{0.95}Ru_{0.05}O_2$ solid solution showed higher resistance values when compared to CeO_2 (1×10^{11} ohms vs. 1×10^9 ohms, see Fig. 7). The resistance increases linearly as a function of gas concentration for the $Ce_{0.95}Ru_{0.05}O_2$ compound. After four cycles, the sample showed an adequate response with a good stability and sensorial properties. Gas response (S) tests performed at lower concentrations (1–5 ppm) show the R_{gas}/R_{air} ratio ranging from 10 to 75. The greater response value was detected for temperature between 200°C and 250°C, which is consistent with values obtained for cerium oxide. These
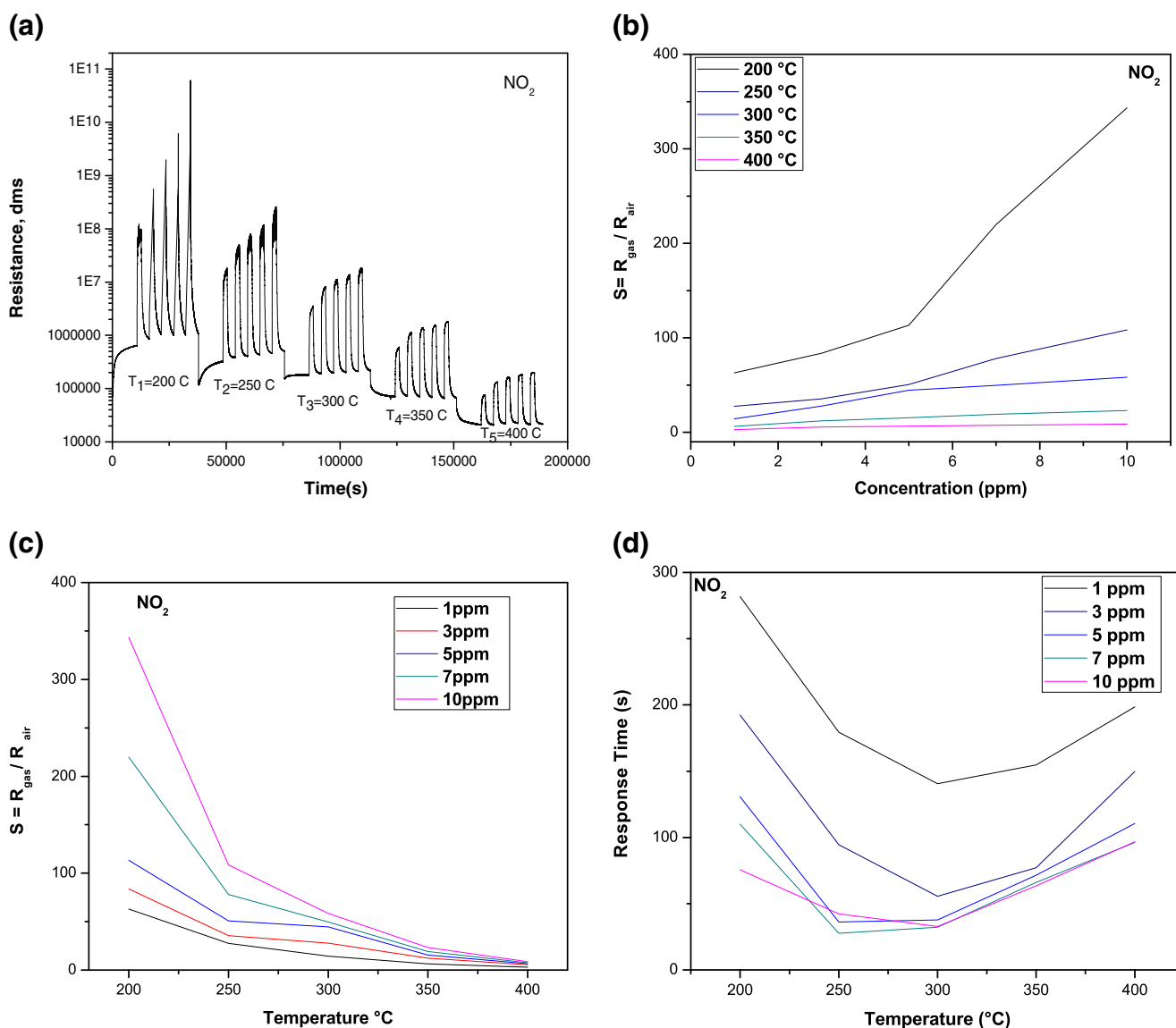
(a)

(b)

(c)

(d)

Fig. 7 $Ce_{0.95}Ru_{0.05}O_2$ graphs for **(a)** Resistance vs time, **(b)** Sensor response vs concentation, **(c)** Sensor response vs temperature, **(e)** Response time vs temperature

results evidence that ruthenium inclusion increased the CeO_2 gas response to a great extent, S=1.8 for CeO_2 vs. S=350 for $Ce_{0.95}Ru_{0.05}O_2$. To our knowledge, no other work regarding this behavior has been reported at the present time.

Concerning the response time, values among 150 and 280 s at concentrations of 1–3 ppm at 200°C were found. In the range of 250 to 350°C, the response time decreases to values as small as 25 s. On the other hand, the recovery time registered values among 150 and 450 s at low temperatures. Save for some minor deviations, the recovery times are within a narrow range among 200 and 300 s.

For the solid $Ce_{0.95}In_{0.05}O_2$ compound (see Fig. 8), their resistance values showed good sensorial response as a function of time, under different concentrations. The material was tested for five cycles, exceeding 300 h without meaningful

saturation. This material shows gas response values ranging from 1 to 10 at low concentrations (1–5 ppm). However, for higher concentrations (7–10 ppm) and temperatures of 300 and 350°C, S reaches values of 30 and 15, respectively. Conversely, at 400°C, the gas response is significantly lower, not higher than S=5 momentarily. This fact is consistent with our previous observations regarding the competition for sites at the surface level. Apparently surface oxygen is depleted at that temperature; however above 400°C, oxygen mobility inside the bulk is increased and gas response and recovery time increase their values. Our discussion is in agreement with the work performed by other authors and will be discussed further.

Therefore, we can establish that $Ce_{0.95}In_{0.05}O_2$ solid solution behaves well in a broad range of working temperatures

(a)

(b)
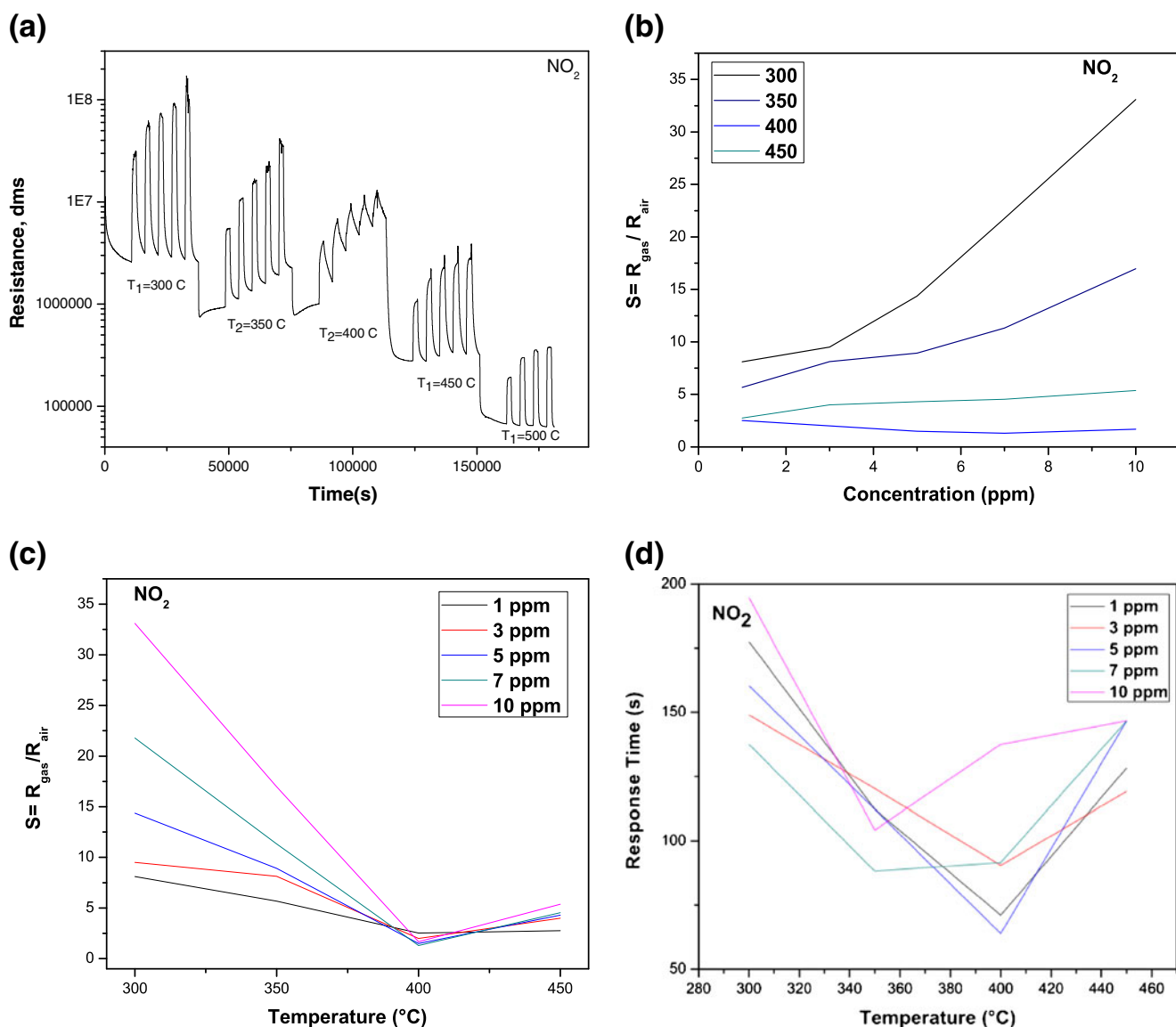

(c)

(d)

Fig. 8 $Ce_{0.95}In_{0.05}O_2$ graphs for **(a)** Resistance vs time, **(b)** Sensor response vs concentation, **(c)** Sensor response vs temperature, **(e)** Response time vs temperature

lower than 400°C for concentration values from 1 to 10 ppm. Response time values are located among 150 and 190 s at the low temperature of 300°C. Between 340°C and 400°C their values are as low as 60 s.

At this point it is pertinent to draw a comparison with published work regarding the development of gas sensors for NO_2. Most reports found in recent literature on gas sensors for NO_2, focus mainly on the study of WO_3 [18], ZnO [19] and SnO_2 [20, 21] compounds, whether in the form of thin films or nanostructures prepared by various methods; and a smaller amount of work addressed to study other sensor compounds, such as In_2O_3 [22]. With respect to cerium oxide as gas sensor there are few studies available in the literature; mostly using ceria as additive. Some of them

relate to the study of CeO_2 as a CO sensor, which seems logical since this compound is currently used in car converters [5–7]. Table 1 shows some results obtained for these compounds relative to NO_2 sensing. As can be seen, the values obtained for our compounds are competitive with those shown by the other authors. Nevertheless, we consider that the values for CeO_2, $Ce_{0.95}Ru_{0.05}O_2$ and $Ce_{0.95}In_{0.05}O_2$ compounds, can be improved once they are tested in the form of thin films. That work is currently under development.

According to the results observed it is possible to establish two working stages of this type of compounds. The explanation is as follows.

At lower temperatures the gas sensing mechanism of cerium oxide belongs to the surface-controlled type in which the

Table 1 Results reported in recent literature for NO$_2$ gas sensors

| Material	Shape	T, (°C) of maximum sensor response	Sensor response	Gas concentration (ppm)	Reference No.
WO$_3$	Nanowires	100–150	1,100	2	17
ZnO	Flowerlike	190	12	0.463	18
ZnO	Tubelike	190	120	0.463	18
SnO$_2$	Hollowspheres	160	2,031	20	19
SnO$_2$	Nanowires	200	180	5	20
In$_2$O$_3$	Microspheres	150	100	100	21
CeO$_2$	Micro fibers	200	1.7	10	This work
Ce$_{0.95}$Ru$_{0.05}$O$_2$	Micro fibers	200–250	350	10	This work
Ce$_{0.95}$In$_{0.05}$O$_2$	Micro fibers	300, 450	35	10	This work

surface states and oxygen adsorption play an important role. Atmospheric oxygen adsorbs electrons from the conduction band of the sensing metal oxide and occurs on the surface in the form of O^-, O_2^- and O_2. The reaction between NO$_2$ and the surface adsorbed species (O_2^-, O- and O_2^-) induces the formation of electron-depleted space-charge layers at the cerium oxide surface and thus the increase in the resistance.

In a second stage, at higher temperature, oxygen increases its mobility within the network of the cerium oxide, rises toward the surface and in this way renews the surface oxygen. Both events are evident in Figs. 6 and 8 and occurring at temperatures of 250 and 400°C, respectively. In this case, indium and ruthenium ions are located in interstitial sites and serve as electron donors as well as oxygen vacancy promoters.

Ceria can be classified as a mixed conductor showing both electronic and ionic conduction. Its electrical properties are strongly dependent upon temperature, oxygen partial pressures and the presence of impurities or dopants [6]. By adding ruthenium or indium to ceria, oxygen vacancies (ionic defects) are promoted since those are related to the appearance of Ce^{3+} ion.

$$Ce^{4+} + Ru^{3+} \leftrightarrow Ce^{3+} + Ru^{4+}$$
$$Ce^{4+} + In^{3+} \leftrightarrow Ce^{3+} + In^{4+}$$
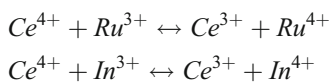
So the formation of Ce$_{1-x}$Ru$_x$O$_{2-y}$ and Ce$_{1-x}$In$_x$O$_{2-y}$ occurs via Ce^{4+} reduction and Ru^{3+} (In^{3+}) oxidation and the corresponding compounds are:

$$Ce_{1-x}^{4+} Ce_x^{3+} Ru_x^{3+} O_y$$
$$Ce_{1-x}^{4+} Ce_x^{3+} In_x^{3+} O_y$$
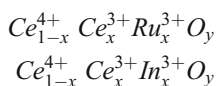
In that case x indicate that the Ru^{3+} addition and Ce^{3+} appearance are closely related and are largely responsible for the significant response found in our materials. However our view is that ruthenium or indium addition are not only stimulating creation of vacancies, but also Ru or In are filling intermediate electronic states between the valence and conduction bands and this allows electron transport

occur more easily. XPS studies are in progress in order to elucidate this assertion.

From the results discussed above, it was demonstrated that the behavior of the Ce$_{0.95}$Ru$_{0.05}$O$_2$ and Ce$_{0.95}$In$_{0.05}$O$_2$ solid solutions is quite different from CeO$_2$. The gas response (S), resistance and recovery time show best values for solid solutions, which evidences that the inclusion of Ru and In has been beneficial. Due to their properties, the CeO$_2$, Ce$_{0.95}$Ru$_{0.05}$O$_2$ and Ce$_{0.95}$In$_{0.05}$O$_2$ systems might be considered in the design of new sensor materials based on oxidation reactions, mainly because the oxidation/reduction process (based on releasing or receiving oxygen), takes place not only at surface level but also inside the lattice.

Further studies are needed, for instance techniques using tagged oxygen; to elucidate the way in which lattice oxygen interacts with NO$_2$ and could be compared to those found by A. Bueno-López et al. [23] using radiotracers. Their studies of the reaction with coal show that oxygen which participates in the oxidation process at temperatures higher than 400°C always comes from the crystallographic network; and although the surface is saturated with labeled oxygen, it does not reacts directly with carbon, demonstrating that the oxygen diffuses from the bulk to the surface to react.

In a recent publication [24] we have addressed the applicability to other gaseous systems, such as carbon monoxide and in addition we are exploring other potential applications as thin films.

5 Conclusions

Significant differences were found by correlating the CeO$_2$ transport properties to the Ce$_{0.95}$Ru$_{0.05}$O$_2$ or Ce$_{0.95}$In$_{0.05}$O$_2$ solid solutions. Ruthenium inclusion increased the CeO$_2$ gas response in a great extent, S=1.8 for CeO$_2$ vs. S=350 for Ce$_{0.95}$Ru$_{0.05}$O$_2$ and S=35 for Ce$_{0.95}$In$_{0.05}$O$_2$. This behavior is reported by the first time. The results demonstrate the direct relationship between morphology, crystal size and cell expansion with the doping material. Ce$_{0.95}$Ru$_{0.05}$O$_2$ and

$Ce_{0.95}In_{0.05}O_2$ form solid solutions without secondary phases (for instance RuO_2 or In_2O_3). Ruthenium or indium doping into CeO_2 keeps the structural framework of the FCC structure. The surface area in mixed oxides is superior to CeO_2, which is attributable to the introduction of dopant. Our findings demonstrate that electronic states added by the inclusion of Ru or In can improve the transport properties of CeO_2. In addition the significant response shown by the solid solutions $Ce_{0.95}Ru_{0.05}O_2$ and $Ce_{0.95}In_{0.05}O_2$ open up the possibilities of application to other gaseous systems like NO, CO and ozone to mention a few.

References

1. N. Yamazoe, G. Sakai, K. Shimanoe, Oxide semiconductor Gas sensors. Cat. Surv. Asia. **7**, 63–75 (2003)

2. N.J. Dayan, S.R. Sainkar, R.N. Karekar, R.C. Aiyer, Formulation and characterization of ZnO:Sb thick-film gas sensors. Thin. Solid Films. **325**, 254–258 (1998)

3. Y. Jianga, N. Bahlawanea, Changes in the structural and optical properties of CeO_2 nanocrystalline films: Effect of film thickness. J. Alloys Comp. **485**, L52–L55 (2009)

4. N. Izu, S. Nishizaki, T. Itoh, M. Nishibori, W. Shin, I. Matsubara, Gas response, response time and selectivity of a resistive CO sensor based on two connected CeO_2 thick films with various particle sizes. Sens. Actuator B. **136**, 364–370 (2009)

5. F. Deganello, A. Martorana, Phase analysis and oxygen storage capacity of ceria-lanthana-based TWC promoters prepared by Sol–Gel routes. J. Solid State Chem. **163**, 527–533 (2002)

6. A. Trovarelli, Catalysis by Ceria and Related Materials, Catalytic Science Series, 1st Ed. (Academic Press inc., 2002).

7. R. Rangel, F. Huerta, P. Bartolo-Pérez, F. Morales-Leal, D. H. Galván, F. Castillón-Barraza, Structural features and catalytic activity of $Ce_{1-x}(La_x, Ru_x)O_2/Bi_2Mo_{0.9}W_{0.1}O_6$, nanostructured solid solutions, in: A. Barrañón (Ed.), (Research in Nanotechnology Developments, Nova Sci. Pub. Inc., 2009), pp. 137–144.

8. W. Chung, Y. Lee, D. Lee, Indium oxide thin film sensors for ozone monitoring produced by a sol-gel method. J. Mat. Sci. Lett. **22**, 907–909 (2003)

9. H.L. Tuller, Defect engineering: Design tools for solid state electrochemical devices. Electrochim. Acta **48**, 2879–2887 (2003)

10. M.A. Ulla, E.A. Lombardo, The Mixed Oxides, in *Handbook on the Physics and Chemistry of Rare Earths*, ed. by K.A. Gschneidner Jr., L. Eyring, 2000, pp. 75–158

11. M. Suchea, N. Katsarakis, S. Chistoulakis, S. Nikolopoulou, G. Kiriakidis, Low temperature indium oxide gas sensors. Sens. Actuator B. **118**, 135–141 (2006)

12. H. Shi-Zhen, L. Wei, Che Wen-Zhe, Gas sensitivity of indium oxide. Trans. Non. Met. Soc. China **19**, s80–s82 (2009)

13. S. Kaleemulla, A.S. Reddy, S. Uthanna, P.S. Reddy, Physical properties of In_2O_3 thin films prepared at various oxygen partial pressures. J. Alloys Compounds. **479**, 589–593 (2009)

14. J. Liu, T. Luo, F. Meng, K. Qian, Y. Wan, J. Liu, Porous hierarchical In_2O_3 micro-/nanostructures: Preparation, formation mechanism, and their application in gas sensors for noxious volatile organic compound detection. J. Phys. Chem. C **114**, 4887–4894 (2010)

15. B. Pejcic, P. Eadington, A. Ross, Environmental monitoring of hydrocarbons: A chemical sensor perspective. Env. Sci. Tech. **41**, 6333–6342 (2007)

16. O.S. Wolfbeis, Fiber-optic chemical sensors and biosensors. Anal. Chem. **78**, 3859–3874 (2006)

17. A. Weibel, R. Bouchet, F. Boulch, P. Knauth, The big problem of small particles: A comparison of methods for determination of particle size in nanocrystalline anatase powders. Chem. Mater. **17**, 2378–2385 (2005)

18. Y. Qin, W. Shen, X. Li, M. Hu, Effect of annealing on microstructure and NO_2–sensing properties of tungsten nanowires synthesized by solvothermal method. Sens. Actuator B. **155**, 646–652 (2011)

19. M. Chen, Z. Wang, D. Han, F. Hu, G. Guo, High-sensitivity NO_2 gas sensors based on flower-like and tube-like ZnO nanomaterials. Sens. Actuator B. **157**, 565–574 (2011)

20. J. Zhang, S. Wang, Y. Wang, Y. Wang, B. Zhu, H. Xia, X. Guo, S. Zhang, W. Huang, S. Wu, NO_2 sensing performance of SnO_2 hollow-sphere sensor. Sens. Actuator. B. **135**, 610–617 (2009)

21. Y. Choi, I. Hwang, J. Park, K. Choi, J. Park, J. Lee, Novel fabrication of an SnO_2 nanowire gas sensor with high sensitivity. Nanotechnology **19**, 095508 (2008)

22. T. Hyodo, H. Inoue, H. Motomura, K. Matsuo, T. Hashishin, J. Tamaki, Y. Shimizu, M. Egashira, NO_2 sensing properties of macroporous In_2O_3-based powders fabricated by utilizing ultrasonic spray pyrolysis employing polymethylmethacrylate microspheres as a template. Sens. Actuator B. **151**, 265–273 (2010)

23. A. Bueno-López, K. Krishna, M. Makkee, J.A. Moulijn, Active oxygen from CeO_2 and its role in catalysed soot oxidation. Cat. Lett. **99**, 203–205 (2005)

24. R. Rangel, L. Chávez Chávez, M. Meléndrez, P. Bartolo-Pérez, E. Pérez-Tijerina, M. García-Méndez, Ce(1-x)MxO2, {M=Ru, In} solid solutions as novel gas sensors for co detection. J. Nano Res. **14**, 137–145 (2011)